

HD 209621: Abundances of neutron-capture elements^{*}

Aruna Goswami¹, Wako Aoki²

¹*Indian Institute of Astrophysics, Koramangala, Bangalore 560034, India; aruna@iiap.res.in*

²*National Astronomical Observatory, Mitaka, Tokyo, 181-8588 Japan; aoki.wako@nao.ac.jp*

Accepted 2009 December 30; Received 2009 December 24; in original form 2009 October 28

ABSTRACT

High resolution spectra obtained from the Subaru Telescope High Dispersion Spectrograph have been used to update the stellar atmospheric parameters and metallicity of the star HD 209621. We have derived a metallicity of $[\text{Fe}/\text{H}] = -1.93$ for this star, and have found a large enhancement of carbon and of heavy elements, with respect to iron. Updates on the elemental abundances of four s-process elements (Y, Ce, Pr, Nd) along with the first estimates of abundances for a number of other heavy elements (Sr, Zr, Ba, La, Sm, Eu, Er, Pb) are reported. The stellar atmospheric parameters, the effective temperature, T_{eff} , and the surface gravity, $\log g$ (4500 K, 2.0), are determined from LTE analysis using model atmospheres. Estimated $[\text{Ba}/\text{Eu}] = +0.35$, places the star in the group of CEMP-(r+s) stars; however, the s-elements abundance pattern seen in HD 209621 is characteristic of CH stars; notably, the 2nd-peak s-process elements are more enhanced than the first peak s-process elements. HD 209621 is also found to show a large enhancement of the 3rd-peak s-process element lead (Pb) with $[\text{Pb}/\text{Fe}] = +1.88$. The relative contributions of the two neutron-capture processes, r- and s- to the observed abundances are examined using a parametric model based analysis, that hints that the neutron-capture elements in HD 209621 primarily originate in s-process.

Key words: stars: Abundances - stars: Carbon - stars: Late-type - stars: Population II.

1 INTRODUCTION

The population II CH stars with their characteristic properties like iron deficiency and enhancement of carbon and s-process elements can provide strong observational constraints for the theoretical computation of nucleosynthesis at low metallicity. Early-type extrinsic CH stars ($^{12}\text{C}/^{13}\text{C} \leq 10$) are confirmed post-mass-transfer binaries (McClure & Woodworth 1990) in which the companion star is an AGB that evolved to a now invisible white dwarf. The chemical composition of the early type CH stars that are characterized by enhancement of s-process elemental abundances bears signatures of the nucleosynthesis processes operating in low-metallicity companion AGB stars, provided they conserve the surface characteristics of the companion stars. These stars thus form ideal targets for studying the operation of s-process at low metallicity. However, not many studies on CH stars can be found; the few earlier studies available are either limited by the resolution or by the wavelength

range. It is important to update the elemental abundances based on higher resolution spectra; the results obtained for heavy elements Zr, La, Ce, Nd with better spectra in a number of CH stars are found to be very different (van Eck et al. 2003) from those estimated earlier (Vanture 1992c). In the present work we report new results on the chemical composition of HD 209621 (V*HP Peg) listed in the CH star catalogue of Bartkevicius (1996).

The star HD 209621 along with two other CH stars HD 5223 and HD 26 have been used as reference stars for studies on medium resolution spectroscopic analysis of candidate Faint High Latitude Carbon stars from the Hamburg/ESO survey (Goswami 2005, Goswami et al. 2007, Goswami et al. 2009). While fairly detailed abundance analyses are available on the stars HD 26 (Van Eck et al. 2003) and HD 5223 (Goswami et al. 2006) a detailed chemical composition for HD 209621 is lacking. Earlier studies on this object are limited by both resolution as well as wavelength regions. Thus the nature of the distribution of the neutron-capture elements and their abundances for this star are necessary to justify its further use as a reference CH star; the present work accomplished this using a high resolution Subaru spectrum for this star.

^{*} Based on data collected at the Subaru Telescope, which is operated by the National Astronomical Observatory of Japan and at HCT, IAO, Hanle, India

Estimated $^{12}\text{C}/^{13}\text{C} \sim 10$ (Tsuji et al. 1991) places HD 209621 in the group of early-type CH stars. A carbon isotopic ratio of 4 is reported by Climenhaga (1960); Vanture (1992a) estimated this value to be ~ 3 using three spectral features: the $^{12}\text{C}^{13}\text{C}$ isotopic 1-0 Swan bandhead at 4744 Å, a blend of three ^{13}CN lines at 8004 Å, and a ^{13}CN feature at 8036 Å which is also a blend of three ^{13}CN lines. Goswami (2005) reported a carbon isotopic ratio of 8.8 measured on a medium resolution spectrum of this object using molecular band-depths of (1,0) $^{12}\text{C}^{12}\text{C}$ λ 4737 and (1,0) $^{12}\text{C}^{13}\text{C}$ λ 4744.

From a comparison of the star's spectrum (13.5 Å mm^{-1} spectrograms) with that of ϵ Vir, Wallerstein (1969) reported an effective temperature of 4700 K for this object. The comparison star ϵ Vir, is a high proper motion star of spectral type G8 III, with near solar metallicity $[\text{Fe}/\text{H}]=0.15$ (McWilliam 1990). With respect to ϵ Vir, Wallerstein derived a metal-deficiency for HD 209621 by a factor of twenty and an enhancement of the ratios of rare earths to metals by a factor of eight. Despite the low metal abundance and high space velocity (velocity components U, V, W = -69, -332, +176), the star was found to lie to the right and below the vertical or giant branches of the globular clusters (Wallerstein 1969).

Vanture (1992c), adopting an effective temperature of 4700 K from Wallerstein (1969) determined abundances for four s-process elements Y, Ce, Pr and Nd using its spectra at resolution $\lambda/\delta\lambda = 20\,000$, lower than ours ($\lambda/\delta\lambda = 50\,000$). Another objective of the present work is to examine and update the elemental abundances of these four heavy elements and estimate abundances for other heavy elements like Sr, Zr, Ba, La, Sm, Eu, Er, W and Pb.

Details of observation and data reduction are reported in section 2. In section 3, we present *BVRIJHK* photometry and discuss the estimates of the effective temperatures from photometry. Determination of the radial velocity and the stellar atmospheric parameters are discussed in section 4. The elemental abundance results are presented in section 5. A brief discussion on the parametric model analysis of the observed abundances is presented in section 6. Discussion and concluding remarks are drawn in section 7.

2 OBSERVATION AND DATA REDUCTION

High-resolution spectroscopic observations of HD 209621 was carried out with the High Dispersion Spectrograph (HDS) of the 8.2m Subaru Telescope (Noguchi et al. 2002) on 20 July, 2005 at a resolving power of $R \sim 50\,000$. The object spectrum was taken with a 5 minutes exposure. The observed bandpass ran from about 4020 Å to 6775 Å, with a gap of about 75 Å, from 5335 Å to 5410 Å, due to the physical spacing of the CCD detectors. Observations of a Th-Ar hollow cathode lamp, provided the wavelength calibration. Standard spectroscopic reductions (e.g., flat fields, bias subtraction, extraction, and wavelength calibration) were carried out using the IRAF¹ spectroscopic reduction package.

¹ IRAF is distributed by the National Optical Astronomical Observatories, which is operated by the Association for Universities for Research in Astronomy, Inc., under contract to the National Science Foundation

3 PHOTOMETRY AND EFFECTIVE TEMPERATURES

Optical broadband *BVRI* photometry along with near-IR *JHK* photometry from 2MASS (Skrutskie et al. 2006), are listed in Table 3. The reddening estimate for HD 209621, $E(B - V) = 0.09$, is from Sleivyte and Bartkevicius (1990). $B - V$, $U - B$, $R - I$ and $V - I$ values are taken from Platais et al. (2003).

We have used colour-temperature calibrations of Alonso et al. 1996) that relate T_{eff} with various optical and near-IR colours. Estimated uncertainty in the temperature calibrations is ~ 90 K. The Alonso et al. calibrations use Johnson photometric systems for *UBVRI* and use TCS (Telescopio Carlos Sanchez) system for IR colours, J-H and J-K. The necessary transformations between these photometric systems are performed using transformation relations from Carpenter (2001), Bessell and Brett (1988) and Alonso et al. (1996, 1999). The colour-based estimates of T_{eff} agree well within 100 - 200 K except for the temperature estimated from $B - V$ colour. The $B - V$ colour of a star with strong molecular carbon absorption features depends not only on T_{eff} , but also on the metallicity of the star and on the strength of its molecular carbon absorption features, due to the effect of CH molecular absorption in the B band. We have not used the empirical T_{eff} scale for the $B - V$ colour indices. The derived T_{eff} from V-K is ~ 400 K, and from J-H is ~ 250 K less than the adopted spectroscopic T_{eff} derived by imposing Fe I excitation equilibrium, described in the next section. The temperature calibrations from the T_{eff} - ($J - H$) and T_{eff} - ($V - K$) relations involve a metallicity ($[\text{Fe}/\text{H}]$) term. Estimates of T_{eff} at two assumed metallicity values (shown in paranthesis) are listed in Table 4.

4 DESCRIPTION OF THE SPECTRA

The high-resolution spectra of HD 209621 are characterized by closely-spaced molecular absorption lines of CH, CN and the Swan system of C_2 . The continuum is obscured over essentially the entire wavelength region. The spectra of HD 209621 are dominated by the lines of carbon bearing molecules; a few unblended atomic lines were possible to identify only from the regions that are relatively clear of molecular lines. Possible blends between atomic and molecular lines were identified on a line-by-line basis using the solar atlas, CH lines and C_2 Swan band systems line lists of Phillips and Davis (1968) and in consultation with atomic line lists of Kurucz. All lines suspected of being blends were eliminated; a final list of Fe I and Fe II lines considered in the present analysis for the determination of atmospheric parameters and metallicity is given in Table 1. Two spectral regions of the star 5025-5045 and 5165-5185 Å are shown in Figure 1 to illustrate the complexity of the star's spectra. A comparison of the spectral regions with those of HE 1305+0007, a double enhanced star with comparable metallicity ($[\text{Fe}/\text{H}] = -2.05$, Goswami et al. 2006), shows great similarity.

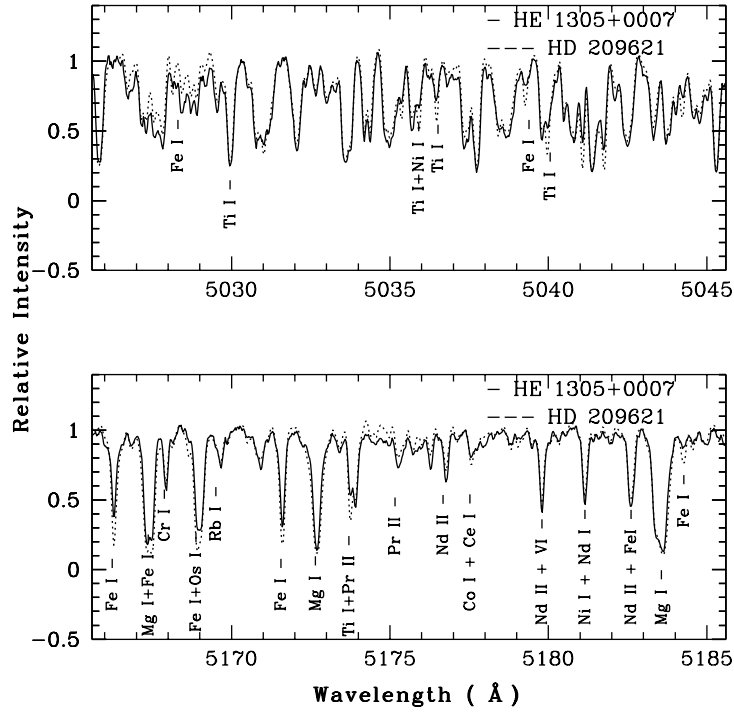


Figure 1. A comparison of the spectra of HD 209621 and HE 1305+0007 in the wavelength region 5025.6 Å to 5045.6 Å (upper panel) and 5165.6 Å to 5185.6 Å (lower panel). A number of prominent lines are indicated on the spectra; the features in HD 209621 closely match their counterparts in HE 1305+0007.

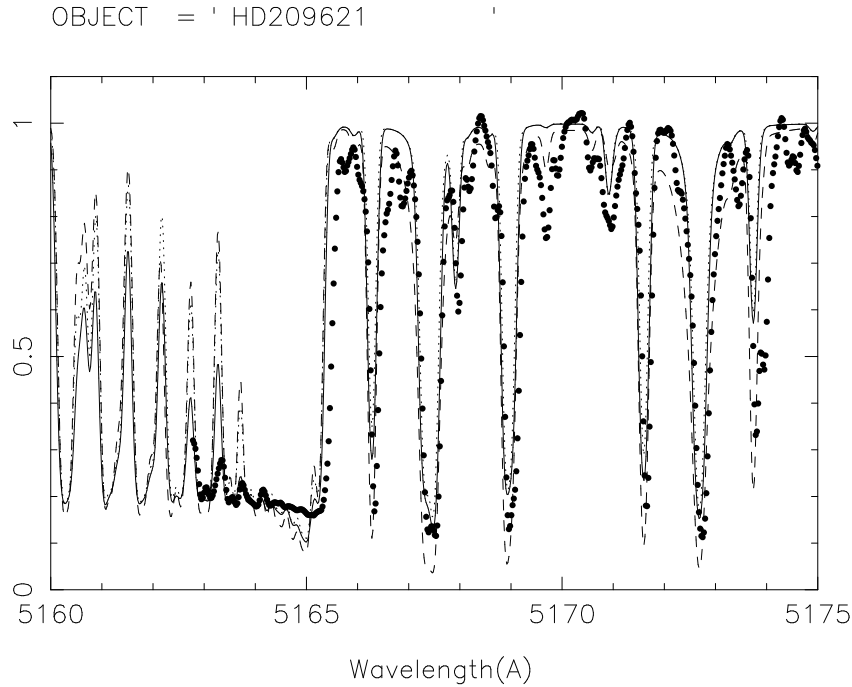


Figure 2. A fit of the synthetic spectrum (dotted curve) compared with the observed spectrum (solid curve) of HD 209621 in the wavelength region 5160 to 5175 Å. The synthetic spectrum is obtained using a model atmosphere corresponding to the adopted parameters listed in Table 5. Calculations made using Vanture's parameters (dashed curve) result in too strong absorptions (in particular Mg line wings).

Table 1: The list of Fe lines used in the present analysis

W_{lab}	ID	EP_{low}	$\log gf$	HD 209621
				Eq widths (mÅ)
6230.726	Fe I	2.5590	-1.281	141.3
6137.694	Fe I	2.5881	-1.403	127.4
6136.615	Fe I	2.4530	-1.400	147.2
5586.760	Fe I	3.3683	-0.210	125.7
5324.178	Fe I	3.211	-0.240	139.0
5324.179	Fe I	3.211	-0.103	139.0
5266.555	Fe I	2.9980	-0.492	138.7
5242.490	Fe I	3.6300	-0.840	64.6
5232.939	Fe I	2.9400	-0.190	154.6
5202.340	Fe I	2.1800	-1.840	134.0
5192.343	Fe I	2.9980	-0.521	124.0
5171.595	Fe I	1.4848	-1.793	174.7
5006.119	Fe I	2.8330	-0.610	134.6
5001.860	Fe I	3.8800	+0.009	80.9
4924.770	Fe I	2.2786	-2.222	94.5
4918.990	Fe I	2.8700	-0.340	139.9
4871.317	Fe I	2.8650	-0.410	142.8
4484.219	Fe I	3.6025	-0.720	66.5
5234.625	Fe II	3.2214	-2.050	74.8
4923.930	Fe II	2.8910	-1.319	144.3
4583.839	Fe II	2.8070	-2.020	93.8
4508.280	Fe II	2.8555	-2.210	60.1

4.1 Radial velocity

We have estimated the radial velocity of HD 209621 using several unblended lines. Estimated heliocentric radial velocity v_r is listed in Table 2. The SIMBAD database lists a mean radial velocity of $v_r = -381 \text{ km s}^{-1}$ for HD 209621. The star is a radial velocity variable. McClure and Woodsworth (1990) determined a period of 407.4 days for this star.

4.2 Stellar atmospheric parameters

The stellar atmospheric parameters, the effective temperature (T_{eff}), the surface gravity ($\log g$), and metallicity ($[\text{Fe}/\text{H}]$) of the star are determined by an LTE analysis of equivalent widths of atomic Fe lines using a recent version of MOOG of Sneden (1973). Eighteen cleanest possible lines of Fe I and four Fe II lines (Table 1) are used in our analysis. Model atmospheres are selected from the Kurucz grid of model atmospheres computed with better opacities and abundances with no convective overshooting. These models are available at <http://cfaku5.cfa.harvard.edu/>, labelled with the suffix “odfnew”. The excitation potentials and oscillator strengths of the lines are taken from various sources, including the Vienna Atomic Line Database (<http://ams.astro.univie.ac.at/vald/>), Kurucz atomic line list (<http://www.cfa.harvard.edu/amp/-ampdata/kurucz23/sekur.html>), Fuhr, Martin, & Wiese (1988), Martin, Fuhr, & Wiese (1988), and Lambert et al. (1996). The gf values of elements compiled by R.E. Luck (private communication) are also consulted.

The effective temperature have also been obtained by the method of excitation balance, forcing the slope of the abundances from Fe I lines versus excitation potential to be near zero. The photometric parameters of HD 209621 are presented in Table 3. The temperature estimates derived

from JHK photometry (Table 4) provided a preliminary temperature check corresponding to which initial model atmosphere is chosen. The effective temperature is then obtained by an iterative process using the method of excitation balance. Estimated T_{eff} is 4500 K. Tsuji et al (1991) derived $T_{\text{eff}} \sim 4400 \text{ K}$ for this object based on Infra Red Flux Method (IRFM), that falls well within the error limits of our temperature determination. We have adopted a microturbulence of 2 km s^{-1} for this star. Such a value is not unrealistic; (in cool giants, with $\log g \leq 2.0$, in general $V_t \geq 2 \text{ km s}^{-1}$ (Vanture 1992c, McWilliam et al. 1995a,b)). Using the Fe I/Fe II ionisation equilibrium, the surface gravity of HD 209621 is obtained as $\log g = 2.0$, same as the value adopted by Tsuji et al. (1991). The metallicity of the star is estimated as $[\text{Fe}/\text{H}] = -1.93$, significantly lower than the metallicity derived by Vanture (1992b, $[\text{Fe}/\text{H}] = -0.9$).

In figure 2, we have shown a fit of the synthetic spectrum (dotted curve) compared with the observed spectrum (solid curve) of HD 209621 in the wavelength region 5163 to 5175 Å. The region is particularly chosen being relatively free from contamination by molecular features. The synthetic spectrum is obtained using a model atmosphere corresponding to the adopted parameters listed in Table 5. Calculations are also made using the set of parameters ($v_t = 3.25$ solid line), changed microturbulence; ($v_t = 2.0$ dotted line) and for Vanture’s parameters; Vanture’s parameters result in too strong absorption (in particular Mg line wings). This indicates that Vanture (1992b) had estimated a higher metallicity for this star. The metallicity derived by us ($[\text{Fe}/\text{H}] \sim -1.93$) is more likely for HD 209621. The atmospheric parameters, the effective temperature and the surface gravity determined by him, however, do not differ much from the ones derived by us. Using $T_{\text{eff}} = 4700 \text{ K}$ of Wallerstein (1969), we could not achieve a satisfactory fit, it

Table 2: Heliocentric Radial velocity v_r of HD 209621

Star Name	v_r km s ⁻¹ our estimation	HJD	v_r km s ⁻¹ from literature
HD 209621	-390.5 ± 1.5	2453541.95451	-381

Table 3: Photometric parameters of HD 209621

Star Name	RA(2000)	Dec(2000)	V	B - V	U - B	R - I	V - I	E(B - V)	J	H	K _s
HD 209621	22 04 25.14	+21 03 09.0	8.86	1.45	1.14	0.61	1.15	0.09	6.661	6.045	5.913

seemed necessary to adopt instead a somewhat lower value for T_{eff} .

From an arithmetic mean of two estimates one ('bolometric') from a reference integrated flux F_0 , the other ('spectral') from calibrated color indices which are representative of Spectral Energy Distributions (SED) shapes, Bergeat et al. (2001) proposed an effective temperature of 4190 K for HD 209621. This value also did not give a satisfactory fit.

The correctness of our estimates is verified by reproducing the atmospheric parameters obtained by Barbay et al. (2005) for the star CS 22948-027. Their estimates are very close to our estimates (refer to Goswami et al. 2006, Table 5). In our analysis that follows, we have adopted $T_{\text{eff}} = 4500$ K, $\log g = 2.0$, and $V_t = 2.0$ km s⁻¹.

5 ABUNDANCE ANALYSIS

Due to severe line blending throughout the spectral range a standard abundance analysis procedure based on the equivalent widths could not be applied for elements other than iron. Therefore, the elemental abundances are derived from spectrum-synthesis calculations. The same method is also applied for all lines irrespective of whether they are affected by hyperfine splitting or not. Local thermodynamic equilibrium is assumed for the spectrum-synthesis calculations. We have used the latest version of MOOG Sneden (1973) for spectrum synthesis. The line list for each region synthesized is taken from the Kurucz atomic line list (<http://www.cfa.harvard.edu/amp/ampdata/kurucz23/sekur.html>) and from the Vienna Atomic Line Database (<http://ams.astro.univie.ac.at/vald/>). Reference solar abundances for the various elemental species are adopted from Asplund, Grevesse & Sauval (2005). The $\log gf$ values for atomic lines are also adopted from Fuhr et al. (1988) and Martin et al. (1988) whenever available, and from a compilation of gf values by R. E. Luck (private communication). For heavy neutron-capture elements $\log gf$ values given by Sneden et al. (1996) and Lawler et al. (2001) are also consulted. The lines used for abundance determination of the elements and their atomic parameters are listed in Table 6. An extended line-list of 248 lines of heavy elements is available (Table 9) as on-line material. Information on the atomic line profiles extracted from the spectrum of HD 209621 has been listed in that table. Table 6 lists only those lines that have been used for abundance determination. The derived abundances are presented in Table 7. In this Table we have listed the abundance $\log \epsilon(X)$, along with $[X/H]$

and $[X/Fe]$ values. In computing the quantity $[X/Fe]$ we have used the Fe I-based abundance for elemental abundances derived from neutral lines and the Fe II-based abundance for elemental abundances derived from ionized lines. Estimated elemental abundances listed in Table 7 are discussed below.

5.1 Carbon, Nitrogen, Oxygen

Carbon (C) Carbon abundance is derived from spectral synthesis of the C₂ Swan 0-1 band around 5635 Å. A synthetic spectrum, derived with an appropriate model atmosphere and using a carbon abundance of $\log \epsilon(C) = 7.7 \pm 0.2$, shows a good match to the depth of the observed spectrum of HD 209621. Relative to the solar photospheric C abundance, C is strongly enhanced in HD 209621 ($[C/Fe] = +1.25$).

The G band of CH is severely saturated in the spectra of HD 209621. This feature is found to be quite insensitive to the carbon abundance. Spectrum synthesis of this feature is likely to return uncertain values and hence we have not considered this band for deriving C abundance. Spectrum synthesis fits of the C₂ Swan 0-1 band around 5635 Å is found to provide reasonable estimate.

Reported C, N, O abundances in HD 209621 by Vanture (1992c) are respectively 8.5, 8.2 and 8.4. Oxygen abundance by Vanture (1992c) is determined from OI near-infrared triplet near 7774 Å applying non-LTE corrections. No clean oxygen lines are detected in our spectra. We have made a rough estimate of oxygen by considering the fact that, the CH stars for which oxygen abundances have been determined follow a particular trend: Oxygen abundance in halo stars are found to increase with decreasing metallicity as $[O/Fe] \sim -0.5 [Fe/H]$ until $[Fe/H] = -1.0$ and then level off at a value of $[O/Fe] = +0.35$ (Wheeler et al. 1989). Based on this we have noted an Oxygen abundance of 7.15 ($\log \epsilon(O) = 7.15$). Also, by assuming the general trend of $[C+N/Fe] = 1$ observed in other CH stars and by using our estimated carbon abundance we have derived the nitrogen abundance as $\log \epsilon(N) = 8.4$. This shows a nitrogen enhancement of $[N/Fe] = +2.5$. Vanture estimated $\log \epsilon(N) = 8.2$, indicating $[N/Fe] = +2.2$.

5.2 The odd-Z elements Na and Al

Sodium (Na) and *Aluminium (Al)* are two monoisotopic, odd elements. Na abundance in HD 209621 is calculated from the resonance doublet - Na I D lines at 5890 Å and 5896 Å. These resonance lines are sensitive to non-LTE effects (Baumüller & Gehren 1997; Baumüller et al. 1998;

Table 4: Estimated effective temperatures (T_{eff}) from semi-empirical relations

Star Name	T_{eff} ($J - K$)	T_{eff} ($J - H$)	T_{eff} ($V - K$)
HD 209621	4205.8	4190.4 (-1.0)	4193.4 (-1.0)
		4223.8 (-2.0)	4102.1 (-2.0)

The numbers inside the parentheses indicate the adopted metallicities [Fe/H]

Cayrel et al. 2004). The derived abundance from an LTE analysis is near solar [Na/Fe] = +0.01.

Observations of Stephens (1999) suggest, Na/Fe decreases with decreasing [Fe/H] from -1 to -2, as expected theoretically. Most other observations available in literature do not support this trend showing instead a flat [Na/Fe] \sim 0 ratio with a large scatter.

Al line at 3961.5 Å which is generally used to derive Al abundances in extremely metal-poor stars is out of the spectral coverage of HD 209621. Other Al lines towards red region are severely blended and could not be used for abundance determination. Although common in Globular clusters enhancement of Na and Al is commonly observed in Globular clusters, but in general, not in field metal-poor stars.

5.3 The α -elements Mg, Si, Ca, and Ti

Magnesium (Mg) The Mg abundance is derived from the synthesis of the Mg I line at 5172.68 Å. The predicted line profile with our adopted Mg abundance ($\log \epsilon(\text{Mg}) = 5.76$) fits the observed line profile in HD 209621 quite well. Magnesium is found to exhibit an overabundance with [Mg/Fe] \sim +0.17.

Silicon (Si) Lines of Si detected in the spectra of HD 209621 are severely blended and could not be used for abundance determination.

Calcium (Ca) The abundance of Ca is derived from the Ca I line at 6102.7 Å. In HD 209621, Calcium abundance gives [Ca/Fe] = +0.08. The Ca abundance is practically as expected for a halo star with [Fe/H] = -2.0 (Goswami & Prantzos 2000, Figure 7).

Titanium (Ti) The Ti abundance derived from the synthesis of the Ti II line at 4805.085 Å shows a marked overabundance of +0.72 with respect to Fe.

5.4 The iron-peak elements Cr, Mn, Ni, Zn

Chromium (Cr) A spectrum synthesis fit of the Cr I line at 5247.566 Å returned an abundance estimate of $\log \epsilon(\text{Cr}) = 3.5$. Cr is mildly deficient with [Cr/Fe] = -0.20. Cr I line at 4254.332 Å with a zero lower excitation potential (E_{low}) is blended with a Ca I line. Lines at 4591.389, 4626.174, 5206.038, 5345.801 Å with similar E_{low} as that of 5247.566 Å appear blended.

Manganese (Mn) No clear good lines due to Mn are detected in the spectra. Mn I lines at 5516.774 Å, 4766.41 Å and 4727.46 Å are detected as blended lines.

Nickel (Ni) The abundance of Ni is derived from a spectrum synthesis calculation of the Ni I line at 5081.107 Å. The measured equivalent width of this line is 37 mÅ. Ni I lines at 5578.711 Å and 5754.655 Å are detected as blended lines. Nickel exhibits a near solar abundance of [Ni/Fe] = -0.01.

Zinc (Zn) The Zn abundance is derived from a spectrum synthesis calculation of Zn I line at 4810.528 Å. Zn is found to be mildly enhanced with [Zn/Fe] = 0.24.

5.5 The light s-process elements Sr, Y, and Zr

Strontium (Sr) The Sr abundance is derived from Sr I line at 4607.327 Å. Sr shows an overabundance of [Sr/Fe] = +1.02; $\log gf$ value (-0.57) for this line is taken from Corliss and Bozman (1962). If we adopt a $\log gf$ value of +0.28 (Snedden et al. 1996) for this line we derive a near-solar abundance for Sr with [Sr/Fe] = +0.08.

Yttrium (Y) The abundance of Y is derived from 5200.41 Å line; Y shows an overabundance of [Y/Fe] = +0.36. Our adopted $\log gf$ value for this line is same as used by Sneden et al. (1996).

Zirconium (Zr) The abundance of Zr is derived using Zr I line at 6134.57 Å. Zr shows an overabundance of [Zr/Fe] = +1.80. $\log gf$ value for this line is taken from Biemont et al. (1981).

Spectrum synthesis fits of Sr, Y and Zr are shown in Figure 3. A discussion on the line selection of the light s-process elements are provided in APPENDIX - A.

5.6 The heavy n -capture elements: Ba, La, Ce, Pr, Nd, Sm, Eu, Er, W, Pb

The abundances of the heavy n -capture elements barium (Ba), lanthanum (La), cerium (Ce), neodymium (Nd), samarium (Sm), praseodymium (Pr), europium (Eu), erbium (Er), tungsten (W) and lead (Pb) are determined using spectrum-synthesis calculations. Spectrum synthesis fits for Ba, La, Nd and Sm are shown in figure 4. The derived abundances are generally found to be overabundant with respect to Fe. Hyperfine-splitting corrections for Y, Ce, and Nd lines are not used. The abundances are not expected to be affected by hyperfine splitting when derived from weak lines (McWilliam et al. 1995a, b). Line selection of the heavy n -capture elements for abundance determination is discussed in APPENDIX - A.

Barium (Ba) The Ba II line at 6141.727 Å is used to determine the Ba abundance. Although broad, this line appears as a well defined symmetric line compared to the other barium lines detected in the spectrum. $\log gf$ value for this line is taken from Miles and Wiese (1969).

Lanthanum (La) The abundance of La is derived from a spectrum-synthesis calculation of the La II line at 5259.38 Å, with atomic data taken from Lawler et al. (2001). La exhibits an overabundance of [La/Fe] = +2.41.

Cerium (Ce) The abundance of Ce is derived from a spectrum-synthesis calculation of the Ce II line at 5274.23 Å. Ce exhibits a large overabundance of [Ce/Fe] = +2.04; this

value is lower than $(+2.8 \pm 0.3)$ derived for Ce by Vanture (1992c).

Praeseodymium (Pr) The abundance of Pr is derived using Pr II line at 5259.7 Å; Pr too exhibits a large overabundance of $[\text{Pr}/\text{Fe}] = +2.16$. This estimate is similar to the value of $+2.2 \pm 0.7$ derived for Pr by Vanture (1992c).

Neodymium (Nd) The abundance of Nd is derived using the Nd II line at 5825.85 Å; Neodymium shows overabundance with $[\text{Nd}/\text{Fe}] = +1.87$; this value is also lower than Vanture’s estimate of $+2.4 \pm 0.6$.

Samarium (Sm) The abundance of Sm is derived from the Sm II line at 4791.60 Å. The $\log gf$ value is taken from Lawler et al. (2006). Sm exhibits an overabundance of $[\text{Sm}/\text{Fe}] = +1.84$.

Europium (Eu) The abundance of Eu is determined from the red line at 6437.64 Å. Eu is overabundant with $[\text{Eu}/\text{Fe}] = +1.35$.

Erbium (Er) The abundance of Er is estimated using Er II line at 4759.671 Å. The line parameters adopted from Kurucz atomic line list come from Meggers et al. (1975). Er shows an overabundance with $[\text{Er}/\text{Fe}] = +2.06$.

Tungsten (W) The abundance of W is determined using the W I line at 4757.542 Å. The line parameters taken from the Kurucz atomic line list come from Obbarius and Kock (1982). The abundance derived is high with $[\text{W}/\text{Fe}] = 2.61$; there is a possible blend with Cr I line at 4757.578 Å (with $\log g$ and lower excitation potential, -0.920 and 3.55 respectively) resulting in an overestimate of W abundance.

Lead (Pb) Spectrum-synthesis calculation is also used to determine the abundance of Pb using the Pb I line at 4057.8 Å. Pb shows an overabundance with $[\text{Pb}/\text{Fe}] = +1.88$.

5.7 Error Analysis

Random errors and systemic errors are the two main sources of errors affecting the derived abundances. Random errors arise due to uncertainties in line parameters, i.e. the adopted gf values and the equivalent width measurements. These errors cause line-to-line scatter in derived abundances for a given species. Random errors are minimized by employing as many usable lines as possible for a given element. In deriving the Fe abundances we made use of 17 Fe I lines and 4 Fe II lines in HD 209621. The derived standard deviation σ is defined by $\sigma^2 = [\sum(\chi_i - \chi)^2 / (N - 1)]$, where N is the number of lines used. The values of σ computed from the Fe I lines are ± 0.17 dex in HD 209621. The corresponding value calculated for Fe II lines is ± 0.11 dex. The computed errors for Fe I and Fe II are listed in Table 7.

Systemic errors arise from uncertainties in our adopted atmospheric parameters. The accuracy of the atmospheric parameters was estimated by computing a set of Fe I lines for pairs of models with (a) the same gravity and microturbulence velocity but different temperatures (b) with the same temperature and gravity but different microturbulence velocities and (c) with the same temperature and microturbulence velocity but different gravities. Variations in the computed equivalent widths from the three cases are compared with the accuracy of equivalent width measurements. This comparison allowed us to estimate the uncertainties in the determination of the atmospheric parameters. The (conservative) uncertainties in the estimated T_{eff} is $\pm 250\text{K}$,

in surface gravity ($\log g$) ± 0.25 dex, and in microturbulence velocity (V_t) ± 0.25 km s⁻¹. Errors in the abundances arising from the errors in atmospheric parameters are not a simple sum of the errors due to the individual parameters. These parameters interact with one another and a change in one may cause a shift in another. The net effect on the derived mean abundances should be considerably less, because we employ the principle of consistency wherein the lines with a large range of excitation potentials, equivalent widths, and different ionization states should lead us to the same value of abundances. In Goswami et al. (2006, Table 8), we have shown the derived differential abundances of elements with respect to those obtained from the adopted model for HE 1305+0007, by varying T_{eff} by ± 250 K, $\log g$ by 0.50 dex, and V_t by 0.25 km s⁻¹.

Except for Fe abundance, the abundances of all the elements listed in Table 7 are derived by spectrum synthesis calculations where we have visually estimated the fitting errors. Our estimated fitting errors range between 0.1 dex and 0.3 dex. We adopt these fitting errors as estimates of the random errors associated with the derived elemental abundances. In Figures 2, 3 and 4 we have shown synthetic spectra for the adopted elemental abundances compared with the synthetic spectra due to two other possible abundances with ± 0.3 dex (see figure captions) differences with respect to our adopted abundances.

6 PARAMETRIC MODEL ANALYSIS OF THE OBSERVED ABUNDANCES

To understand the nucleosynthetic origin of the heavy elements it is important to know the relative contributions from the s- and r-process to their observed abundances. We have examined the relative contributions of these two processes by comparing the observed abundances with predicted s- and r-process contributions in the framework of a parametric model for s-process (Howard et al. 1986). This model was also used by many (Aoki et al. 2001, Bo Zhang et al. 2006) to study the s-process element abundances in very metal-poor stars. We have used the solar system isotopic abundances (both s- and r-process) given in Arlandini et al. (1999). The solar system r- and s- process elemental abundances derived from the isotopic abundances are scaled to the metallicity of the star. These values (logarithmic with base 10) are normalized to the observed Ba abundance of the corresponding stars.

We have used the following two parametric model functions

$$N_i(Z) = A_s N_{s,i} + A_r N_{r,i} \quad (\text{A})$$

$$N_i(Z) = A_s N_{s,i} + (1 - A_s) N_{r,i} \quad (\text{B})$$

where Z is the metallicity of the star $N_{s,i}$ is the i th element abundance produced by s-process, $N_{r,i}$ is the i th element abundance produced by r-process.

The coefficients A_s and A_r obtained from non-linear least square fits represent the contributions coming from s- and r-process respectively. The model fits obtained using model function (A) are shown in figure 5. The derived co-

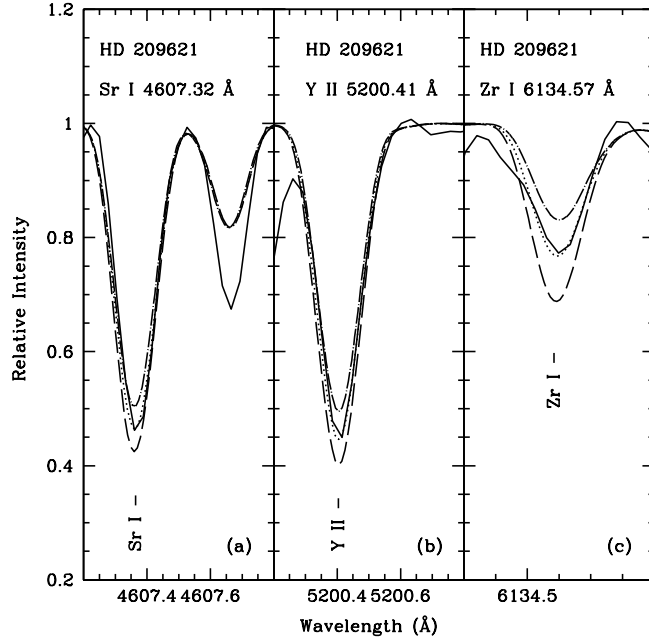


Figure 3. Spectral-synthesis fits of absorption lines arising from the light s-process elements Sr, Y, and Zr, obtained with the elemental abundances listed in Table 7. The dotted lines indicate the synthesized spectra and the solid lines indicate the observed line profiles. Two alternative synthetic spectra for $\Delta[X/Fe] = +0.3$ (long dash) and $\Delta[X/Fe] = -0.3$ (dot-dash) are shown to demonstrate the sensitivity of the line strength to the abundances.

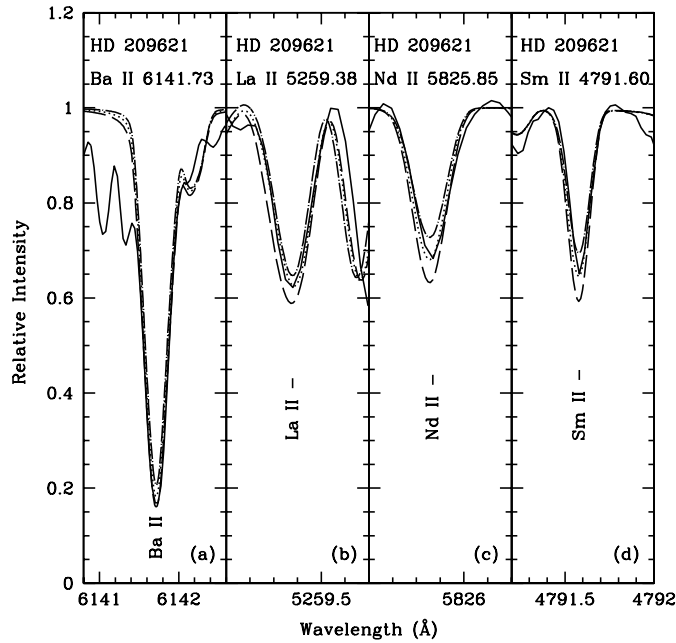


Figure 4. Spectral-synthesis fits of absorption lines arising from the heavy s-process elements Ba, La, Nd, and Sm, obtained with the respective elemental abundances listed in Table 7. The dotted lines indicate the synthesized spectra and the solid lines indicate the observed line profiles. Two alternative synthetic spectra for $\Delta[X/Fe] = +0.3$ (long dash) and $\Delta[X/Fe] = -0.3$ (dot-dash) are shown to demonstrate the sensitivity of the line strength to the abundances.

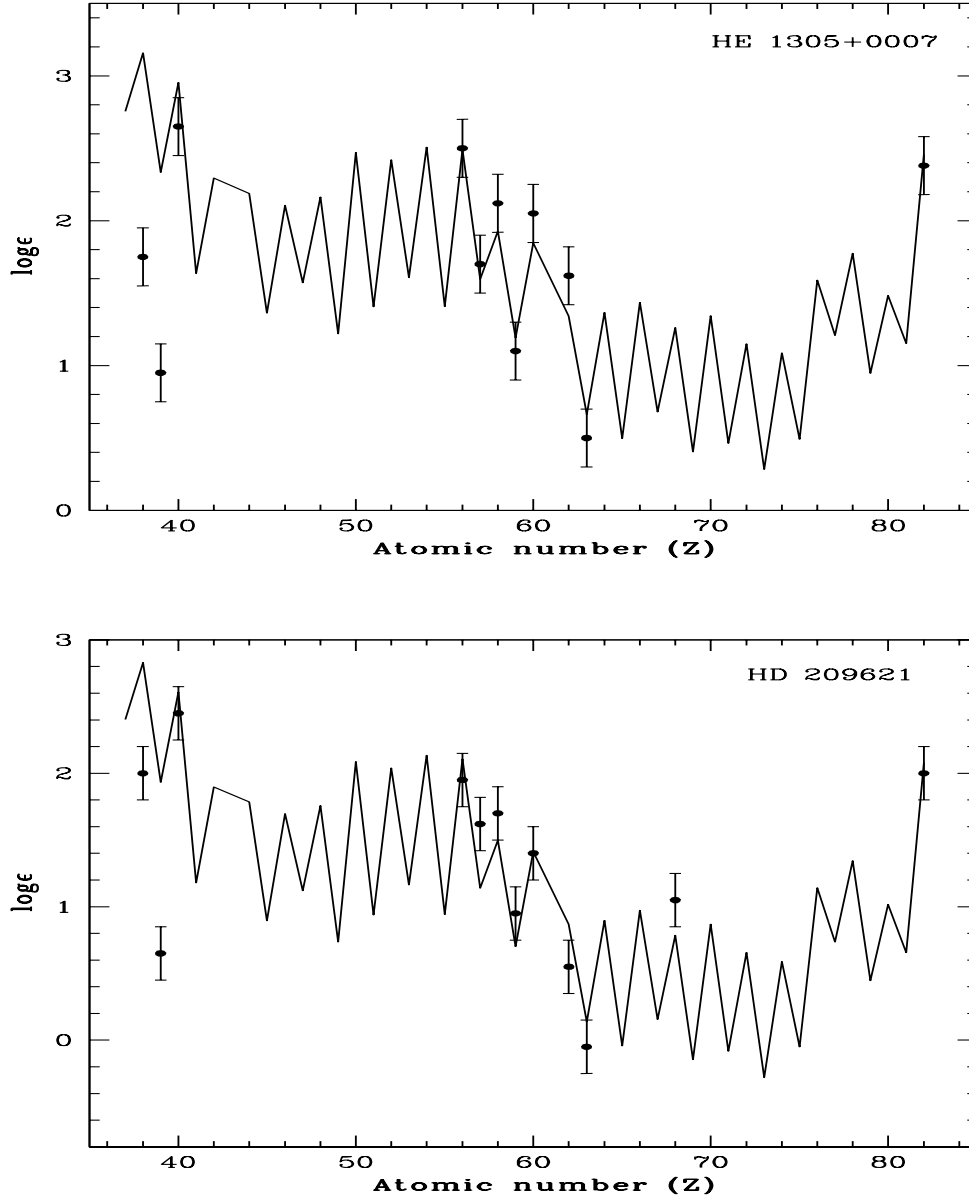


Figure 5. Solid curves represent the best fit for the parametric model function $\log \epsilon = A_s N_{si} + A_r N_{ri}$, where N_{si} and N_{ri} represent the abundances due to s- and r-process respectively (Arlandini et al. 1999, Stellar model, scaled to the metallicity of the star). The best fit coefficients A_s , A_r and their respective reduced chisquare are listed in Table 8. The points with errorbars indicate the observed abundances in HE 1305+0007 (upper panel) and HD209621 (lower panel).

efficients A_s , A_r and the reduced chisquare (χ^2_ν) values for HD 209621 are listed in table 8. These values obtained for HE 1305+0007 is also listed in table 8 for comparison. The abundances of neutron-capture elements for HE 1305+0007 are adopted from Goswami et al. (2006). The 1st peak elements Sr, Y and Zr are not included in the fitting as they are not abundantly produced as 2nd peak ones by the s-process in metal-poor AGB stars in general. The contributions of r- and s-process elements are estimated from the fitting for Ba-Eu.

Calculated coefficients for HE 1305+0007 indicate that contribution from the r-process is higher than the contribution from s-process; this supports placing of HE 1305+0007

in CEMP-r+s group. In case of HD 209621, estimated A_s is slightly higher than A_r indicating the dominance of s-process in the observed abundances. It is noticed in Figure 6, that the abundance pattern of elements $56 \leq Z \leq 63$ agree with the s-process pattern much better than with the r-process. It is to be noted that, although [Ba/Eu] estimate places HD 209621 in the group of the CEMP-r+s stars; La/Eu and Ce/Eu are high and that can be explained by s-process models.

Table 5: Derived atmospheric parameters

Star Names	T_{eff}	$\log g$	V_t km s $^{-1}$	[Fe I/H]	[Fe II/H]
HD 209621	4500	2.0	2.0	-1.94	-1.92
CS 22948-027	4750	1.5	2.0	-2.50	-2.40
HE 1305+0007 ^a	4750	2.0	2.0	-2.03	-1.99

^a from Goswami et al. (2006)

Table 6: Lines used for abundance determination

W_{lab}	Z	ID	EP_{low}	$\log gf$	Remarks
5889.951	11.0	Na I	0.00	0.117	syn
5895.932	11.0	Na I	0.00	-0.184	syn
5172.684	12.0	Mg I	2.712	-0.402	syn
6155.693	14.0	Si I	5.619	-1.690	syn
6102.723	20.0	Ca I	1.879	-0.890	syn
4415.559	21.1	Sc II	0.595	-0.640	syn
4805.090	22.1	Ti II	2.061	-1.100	syn
5247.566	24.0	Cr I	0.961	-1.640	syn
5081.107	28.0	Ni I	3.847	+0.300	syn
4810.528	30.0	Zn I	4.078	-0.137	syn, 'as rw'
4607.327	38.0	Sr I	0.000	-0.570	syn
5200.413	39.1	Y II	0.992	-0.569	syn
6134.585	40.0	Zr I	0.000	-1.280	syn, 'as lw'
6141.727	56.1	Ba II	0.704	-0.076	syn
5259.380	57.1	La II	0.173	-1.760	syn, shallow
5274.229	58.1	Ce II	1.044	0.323	syn
5259.728	59.1	Pr II	0.633	0.080	syn, shallow
5825.857	60.1	Nd II	1.081	-0.760	syn
4791.580	62.1	Sm II	0.104	-1.44	syn
6437.640	63.1	Eu II	1.319	-0.276	syn, shallow
4759.653	68.0	Er II	0.000	-1.904	syn
4757.542	74.0	W I	0.366	-2.430	syn
4057.807	82.0	Pb I	1.320	-0.170	syn, 'as'

“syn” indicates abundances are derived from spectrum synthesis

“as lw” indicates asymmetry in the left wing

“as rw” indicates asymmetry in the right wing

7 DISCUSSION AND CONCLUDING REMARKS

We confirm HD 209621 to be a highly carbon-enhanced metal-poor star and update earlier estimates of four s-process elements Y, Ce, Pr and Nd by Vanture (1992c). Further, we have obtained error range from 0.1 to 0.3 , much lower compared to those of 0.7 and 0.6 dex respectively for Pr and Nd by Vanture (1992c). New abundance estimates for many other neutron-capture elements such as Sr, Zr, Ba, La, Sm, Eu, Er, W, Pb are presented. The abundance pattern of α elements are found to be similar to those generally seen in halo stars of similar metallicity (McWilliam et al. (1995a, b), Ryan, Norris, & Beers (1996), Cayrel et al. 2004). While in Sun $[\text{Sr}/\text{Ba}] = 0.75$, HD 209621 shows a much smaller ratio with $[\text{Sr}/\text{Ba}] = -0.68$.

HD 209621 shows a larger enhancement of 2nd peak s-process elements (Ba, La, Ce, Nd, Sm) than 1st-peak s-process elements (Sr and Y). The enhancement of s-process elements along with the large enhancement of carbon, indicates a mass-transfer event in a binary system from a companion AGB star that underwent s-process nucleosynthesis during its lifetime. The star also shows a large enhancement of Eu similar to those seen in a group of CEMP-(r+s) stars

with $[\text{Ba}/\text{Eu}] \geq 0$. Thus HD 209621 shows characteristics of both CH and CEMP-(r+s) stars: in terms of enhancement of heavy s-process elements relative to the lighter s-process elements it shows characteristics of CH star and estimated $[\text{Ba}/\text{Eu}] = +0.35$ places the star in the group of CEMP-(r+s) stars. In Figure 7, we have plotted $[\text{Ba}/\text{Fe}]$ vs $[\text{Eu}/\text{Fe}]$ for stars belonging to different classes of CEMP stars. Different classes of CEMP stars are seen to be well separated in the $[\text{Ba}/\text{Fe}]$ vs $[\text{Eu}/\text{Fe}]$ plot. The locations of HD 209621 as well as of HE 1305+0007 fall well within the region occupied by (r+s) stars supporting their classification as (r+s) stars. The chemical homogeneity within the (r+s) group with a clear separation from r- and s-stars is interesting.

HD 209621 also shows a large enhancement of the 3rd-peak s-process element lead ($[\text{Pb}/\text{Fe}] = +1.88$). The enhanced Eu abundance, together with the large abundance of the 3rd-peak s-process element Pb indicate a coupling of high s-process and high r-process enrichment. Enhancement of Pb abundance is noticed in a number of CH as well as CEMP-(r+s) stars. Van Eck et al. (2003) defined stars with $[\text{Pb}/\text{hs}] \geq +1.0$ as ‘lead stars’, where hs includes Ba, La and Ce. According to a simplified definition by Jonsell et al. (2006) ‘lead stars’ are those with $[\text{Pb}/\text{Ba}] \geq 1.0$. The latter definition does not require the ‘lead stars’ also to be (r+s)

Table 7: Chemical composition of HD 209621

Element	Z	Solar ^a log ϵ	HD 209621 log ϵ	[X/H]	[X/Fe]	Ref [X/Fe]	[X/Ba]
C	6	8.39	7.7	-0.69	+1.25	+2.29	-0.47
Na I D ₂	11	6.17	4.10	-2.07	-0.13	—	-1.85
Na I D ₁	11	6.17	4.40	-1.77	+0.15	—	-1.55
Mg I	12	7.53	5.76	-1.77	+0.17	—	-1.55
Ca I	20	6.31	4.45	-1.86	+0.08	—	-1.64
Sc II	21	3.05	1.92	-1.13	+0.79	—	-0.91
Ti II	22	4.9	3.70	-1.20	+0.72	—	-0.98
Cr I	24	5.64	3.50	-2.14	-0.20	—	-1.92
Fe I	26	7.45	5.51±0.17	-1.94	—	—	-1.72
Fe II	26	7.45	5.53±0.11	-1.92	—	—	-1.70
Ni I	28	6.23	4.28	-1.95	-0.01	—	-1.73
Zn I	30	4.60	2.90	-1.70	+0.24	—	-1.48
Sr I	38	2.92	2.0	-0.92	+1.02	+1.1±0.3	-0.70
Y II	39	2.21	0.65	-1.56	+0.36	—	-1.34
Zr I	40	2.59	2.45	-0.14	+1.80	—	+0.08
Ba II	56	2.17	1.95	-0.22	+1.70	—	—
La II	57	1.13	1.62	+0.49	+2.41	—	+0.71
Ce II	58	1.58	1.70	+0.12	+2.04	+2.8±0.3	+0.34
Pr II	59	0.71	0.95	+0.24	+2.16	+2.2±0.7	+0.46
Nd II	60	1.45	1.40	-0.05	+1.87	+2.4±0.6	+0.17
Sm II	62	1.01	0.55	-0.46	+1.46	—	-0.24
Eu II	63	0.52	-0.05	-0.57	+1.35	—	-0.35
Er II	68	0.93	1.05	+0.12	+2.06	—	+0.34
W I	74	1.11	1.78	+0.67	+2.61	—	+0.89
Pb I	82	2.00	1.94	-0.06	+1.88	—	+0.16

^a Asplund, Grevesse & Sauval (2005); Ref: Vanture (1992c)

Table 8 : Coefficients and reduced χ^2_ν for the parametric model $N_i(Z) = A_s N_{s,i} + A_r N_{r,i}$

Objects	[Fe/H]	A _s	A _r	χ^2_ν
HE 1305+0007	-2.0	0.469± 0.11	0.528±0.09	1.07
HD 209621	-1.94	0.568± 0.10	0.518±0.08	1.80

stars, but requires that they are enhanced in Ba and Pb, and much more in the latter element. In HD 209621, although we find an enhanced abundance of Pb, [Pb/Ba] is found to be less than +1.0 and hence according to the above definitions HD 209621 does not belong to the group of ‘lead stars’. Aoki et al. (2001) also found metal-poor stars, LP 625-44 and LP 706-7, to be enriched in s-process elements including Pb but cannot be considered as lead stars ([Pb/Ce] ≤ 0.4). In figure 8, we compare the abundances of HD 209621 with the abundances of CS 22948-027, CS 22497-034 (Hill et al. 2000, Barbuy et al. 2005) and HE 1305+0007 (Goswami et al. 2006). These three stars show large enhancement of Carbon, and both r- and s- process elements, including Pb. The atmospheric parameters, metallicities, and heavy-element abundance patterns of these three objects are very similar to HD 209621. Although binarity of HE 1305+0007 is not yet established, both the CS stars and HD 209621 are known to be long-period binaries (Preston and Sneden 2001, Barbuy et al. 2005, McClure and Woodsworth 1990). From the figure it is evident that Pb shows a distinct trend with metallicity in these objects. From the similarity in the abundances, it is also likely that these objects form a group originating from a similar physical scenario.

According to the CEMP stars taxonomy of Beers and Christlieb (2005), (r/s) stars are defined by limits on s-elements as [Ba/Fe] ≥ +1.0 and r-element as [Ba/Eu] ≤

0.5 with [Eu/Fe] ≥ +1.0. A criteria [Ba/Eu] ≥ 0.0 is set for (r+s) stars (Jonsell et al. 2006) which overlaps with the class of ‘r/s stars’. Beers & Christlieb, define s-stars as having [Ba/Fe] > +1.0 and [Ba/Eu] > +0.5. The s-stars are often C rich (Jonsell et al. 2006, Table 8), while the r stars are generally less C rich. It is not clear, however, if all (r+s) stars are also CH stars, although all 17 (r+s) stars listed by Jonsell et al. have considerably enhanced carbon abundances. However, a relatively high fraction of the CH stars seem to be (r+s) stars (e.g. Aoki et al. 2002). According to Abia et al. (2002), CH stars cannot be formed above a threshold metallicity, around $Z \sim 0.4Z_{M\odot}$; the observed CEMP-(r+s) are found to lie within a metallicity range -2.0 (HE 1305+0007, Goswami et al. 2006) and -3.12 (CS 22183-015, Johnson and Bolte 2002). The majority of (r+s) stars listed by Jonsell et al. are turn-off point stars while CH stars are known to be giants.

In order to understand the origin of neutron-capture elements, the resulting abundances of neutron capture elements for HD 209621 are plotted (figure 6) along with the scaled abundance patterns of the solar system material, the main s-process component, and the r-process pattern (Arlandini et al. 1999). The abundance patterns of elements with $56 \leq Z \leq 63$ agree with the s -process pattern much better than with the r-process pattern indicating that the neutron-capture elements in HD 209621 principally originate in the

s-process. Estimated $[\text{Ba}/\text{Eu}]$ ($= +0.35$) for HD 209621 is significantly lower than that seen in the main s-process component ($[\text{Ba}/\text{Eu}] = 1.15$, Arlandini et al. 1999). Such low values for $[\text{Ba}/\text{Eu}]$ were also noticed in stars CS 29526-110, CS 22898-027, CS 31062-012, and CS 31062-050; the ratios $[\text{Ba}/\text{Eu}]$, for these objects range from 0.36 to 0.47. The abundance patterns of elements $56 \leq Z \leq 63$ are however in agreement with the s-process pattern (Aoki et al. 2002). The observed low values of $[\text{Ba}/\text{Eu}]$ in the four CS stars are interpreted as a result of an s-process that produces different abundance ratios from that of the main s-process component (Aoki et al. 2002). This interpretation is supported by models of Goriely & Mowlavi (2000) that predicted $[\text{Ba}/\text{Eu}] = 0.4$ for yields of metal-deficient AGB stars. A similar interpretation also seems applicable to HD 209621; the abundance pattern observed in HD 209621 as being produced by s-process although r-process contamination may have contributed to the observed Eu excesses to some extent. Analysis of the observed abundances of the heavy elements with parametric model function (A) also shows that s-process have slightly higher contributions with $A_s = 0.56$ than r-process with $A_r = 0.51$, where A_s and A_r are the component coefficients that correspond to contributions from the s- and r-process respectively. Here, the contributions from r- and s-process are estimated from the fitting for Ba - Er.

A widely accepted scenario for the formation of CH stars, known to be single-line spectroscopic binaries is the mass transfer from a companion AGB star (McClure 1983, 1984 and McClure and Woodsworth 1990). Temporal variations of radial velocities observed among the known CH stars indicate binarity of the objects. McClure and Woodsworth (1990) have noted the star HD 209621 to be a radial velocity variable with a period of 407.4 days. Our estimated radial-velocity ($-390 \pm 1.5 \text{ km s}^{-1}$) also indicates that HD 209621 is a high-velocity star and a likely member of the Galactic halo population. Such high velocities are a common feature of CH stars. These properties also point towards the fact, that the observed enhancement of neutron-capture elements in HD 209621 resulted from a transfer of material rich in s-process elements across a binary system with an AGB star. The abundance ratios of neutron-capture elements in HD 209621 shown by the present study underscores the need for detailed studies of a larger sample of CH stars in order to develop a comprehensive scenario for the production of heavy-elements by the s-process operating at low metallicity. Such studies are also likely to provide with clues to the limit on the metallicity of stars that show double enhancement.

Acknowledgements

We are grateful to the referee Professor Chris Sneden, for his constructive suggestions, which have improved the readability of the paper considerably. We would like to thank Drisyra Karinkuzhi for figs 5 and 6. This work made use of the SIMBAD astronomical database, operated at CDS, Strasbourg, France, and the NASA ADS, USA. Funding from the DST Project No. SR/S2/HEP-09/2007 is gratefully acknowledged.

APPENDIX - A

Strontium (Sr) The Sr abundance is derived from Sr I line

at 4607.327 Å. Sr II line at 4077.7 Å is detected as a blended line. Absorption tip of Sr II line at 4215.52 Å is also identified. This line is blended with contributions from the CN molecular band around 4215 Å. Sr II line at 4161.82 Å could not be detected in our spectrum. Sr I line at 6550.24 Å is blended with a Sc II line.

Yttrium (Y) The abundance of Y is derived from 5200.41 Å line. Y II line at 4398.1 Å is asymmetric on the right wing, probably blended with a Nd II line at 4398.013 Å and could not be used for abundance determination. Y II line at 4883.69 Å is also asymmetric on the right wing, blended with a Sm I line at 4883.777 Å. YII lines at 5087.43 and 5123.22 Å both are detected, while 5087.43 shows asymmetry on the right wing, 5123.22 Å line is detected as a shallow feature, both the wings not reaching the continuum. YII line at 5205.73 Å is also detected as a shallow feature. Y I line at 4982.129 Å is blended with a Mn I line. The line at 5473.388 Å is blended with contributions from Mo I and Ce I lines. Vanture (1992c) estimated Y abundance to be $+1.1 \pm 0.3$. We note that the $\log gf$ value for 5200.41 Å line used by Vanture is -0.49 . This value is different from what we have adopted (-0.569) from Sneden et al. (1996).

Zirconium (Zr) The abundance of Zr is derived using Zr I line at 6134.57 Å. Zr II line at 4496.97 Å appears as a blend with Co I line at 4496.911 Å. Absorption tip of Zr II line at 4161.21 is easily detected. Lines detected at 4208.99, 4258.05 and 4317.32 Å are heavily contaminated by contributions from molecular bands. Zr II line at 4404.75 Å is blended with an Fe I line and the 4317.321 Å line is blended with a Ce II line. None of the Zr II lines are usable for abundance determination.

Barium (Ba) We have used the Ba II line at 6141.727 Å to determine the Ba abundance. Although broad, this line appears as a well defined symmetric line compared to all the other barium lines detected in the spectrum. $\log gf$ value for this line is taken from Miles and Wiese (1969). Ba II line at 4130.65 Å is found to be heavily contaminated by molecular contributions, this line is not considered for abundance determination. Ba II resonance line at 4554 Å is extremely strong and broad, we have excluded this line as well for abundance analysis. Ba II line at 5853.668 Å shows asymmetry in the right wing. Ba II line at 6496.897 Å appears as a broad profile much below the continuum. A single Ba I line that we have detected at 5907.66 Å appears as a broad line and not well defined. We have not used this line for abundance determination.

In the case of Ba the hyperfine-splitting (HFS) corrections depend on the r/s fraction assumed to have contributed to the enrichment of the star. This element has both odd and even isotopes. The odd isotopes are mainly produced by the r-process and have a broad HFS, while the even isotopes are mainly produced by the s-process, and exhibit no HFS. It was shown by Sneden et al. (1996) that this issue is important for the Ba lines at 4554 Å and 4934 Å, and unimportant for the lines at 5854, 6142, and 6497 Å. We have used the red Ba II line at 6141.73 Å. The HFS splitting of this line is $\sim 1/5$ of the Ba 4554 Å splitting and $\sim 1/3$ of the thermal line width, and hence HFS corrections could be neglected. The effect of hyperfine splitting is smaller than 0.02 dex for the 5853 Å and 6141 Å lines (McWilliam et al. 1998). Ba is found to exhibit a marked overabundance of $[\text{Ba}/\text{Fe}] = +1.70$.

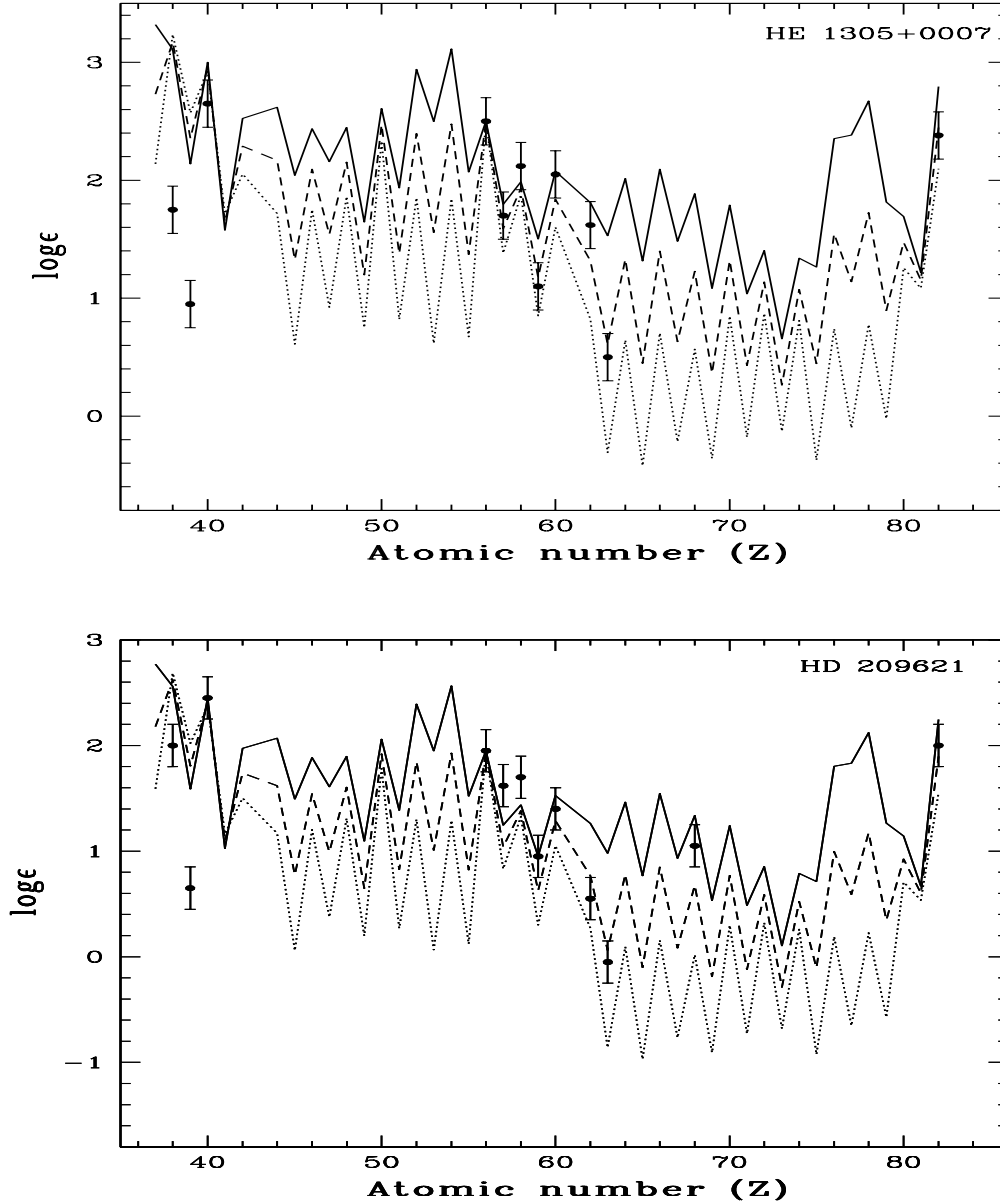


Figure 6. Solid line shows abundances due to only r-process, dotted line of s-process only and dashed line indicates abundance pattern derived from a simple average abundances coming from r- and s- process. The abundances are scaled to the metallicity of the star and normalized to the observed Ba abundances. The points with errorbars indicate the observed abundances in HE 1305+0007 (upper panel) and HD 209621 (lower panel).

Lanthanum (La) The abundance of La is derived from a spectrum-synthesis calculation of the La II line at 5259.38 Å, with atomic data taken from Lawler et al. (2001). La II line at 4123.23 Å is detected as a shallow feature. Absorption tip of La II 4238.38 Å line is detected; this line is contaminated by molecular contributions. A low absorption profile of 4322.51 Å line is also detected, but not found suitable for abundance determination. The line at 4333.7 Å is contaminated by molecular contributions. La II lines at 4429.90 and 4558.46 Å both show asymmetry in their right wings. La II line at 4574.88 Å also appears as an asymmetric broad profile. Traces of La II lines at 4613.39 and 5123.01 Å are detected; low absorption profile of La II lines at 4662.51 Å is

prominently seen. These lines have $E_{low} \sim 0$ eV. Two other zero eV lines at 4086.709 Å and 5808.313 Å are detected as shallow profiles with their wings much below the continuum. 6320.43 Å line shows asymmetry on the right wing.

Cerium (Ce) We have examined seven Ce I and forty five Ce II lines in the spectrum of HD 209621 (Table 9, available on-line); however, they are either affected by molecular contamination or blended with contributions from other elements. The abundance of Ce is derived from spectrum-synthesis calculations of the Ce II line at 5274.23 Å. Ce exhibits a large overabundance of $[Ce/Fe] = +2.04$; this value is lower than Vanture's ($+2.8 \pm 0.3$).

Praesodymium (Pr) Pr I line at 5996.060 Å is detected

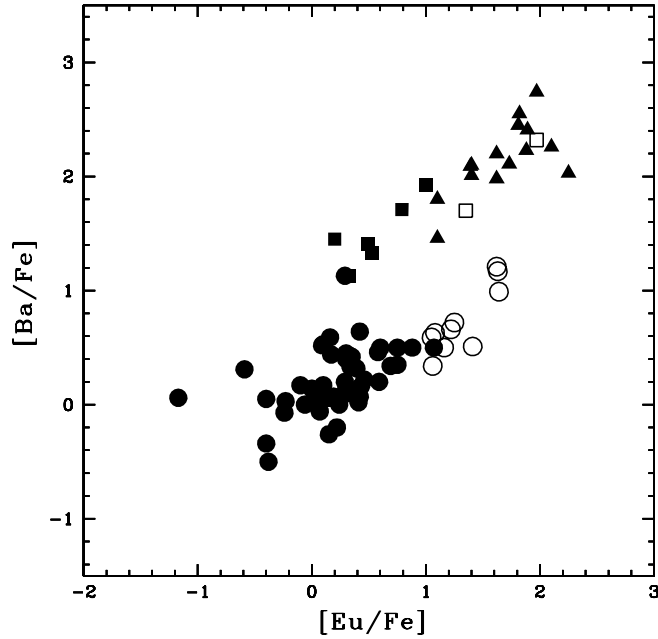


Figure 7. $[\text{Ba}/\text{Fe}]$ vs $[\text{Eu}/\text{Fe}]$ plot for stars of different classes of CEMP stars. The r+s stars are indicated by solid triangles, r stars by open circles, s stars by solid squares and the normal stars that do not show enhancement of either s or r elements are shown with solid circles. Different classes of CEMP stars are seen to be well separated; the location of HE 1305+0007 and HD 209621 shown by open squares are well within the region occupied by r+s stars. The data points are taken from the compilation of Jonsell et al. (2006).

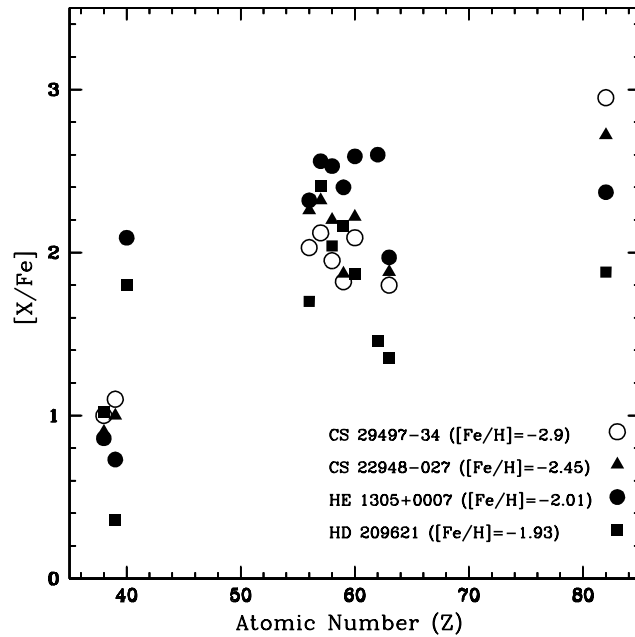


Figure 8. A comparison of the distribution of n-capture elements abundances ($[\text{X}/\text{Fe}]$) versus their atomic numbers (Z) in HD 209621 with those found in CEMP stars CS 29497-34, CS 22948-027, and HE 1305+0007. The later three stars show double enhancement of r- and s- process elements. An interesting feature noticed is the increase in Pb abundances with decreasing metallicities of the stars.

as an asymmetric line. None of the Pr II lines in the wavelength region 4100 - 4500 Å (Table 9) were detected in the spectrum of HD 209621. Pr II line at 5188.217 Å is blended with a La II line and lines at 5219.045 Å and 5220.108 Å appear as asymmetric lines. The Pr II line at 5259.7 Å is used to derive the abundance of Pr. Pr exhibits a large overabundance of $[\text{Pr}/\text{Fe}] = +2.16$. This estimate is similar to the value of $+2.2 \pm 0.7$ derived for Pr by Vanture (1992c).

Neodymium (Nd) Nd I line at 6432.680 Å is detected as a clean line. Forty two Nd II lines listed in Table 9 are examined; most of them are blended with contributions from other elements. The abundance of Nd is derived using the Nd II line at 5825.85 Å; Neodymium shows overabundance with $[\text{Nd}/\text{Fe}] = +1.87$; this value is also lower than Vanture's estimate of $+2.4 \pm 0.6$.

Samarium (Sm) Two Sm I and twenty six Sm II lines have been examined in the spectrum of HD 209621. The abundance of Sm is derived from the Sm II line at 4791.60 Å. There seems to exist no significant contamination of this line. The *log gf* value is taken from Lawler et al. (2006). Sm exhibits an overabundance of $[\text{Sm}/\text{Fe}] = +1.84$.

Europium (Eu) The main lines of Eu that are generally used in abundance analysis are the Eu II lines at 4129.7, 4205.05, 6437.64 and 6645.13 Å. The blue Eu II lines at 4129.7 and 4205.05 Å are severely blended with strong molecular features and could not be used for abundance analysis. The abundance of Eu is therefore determined from the red line at 6437.64 Å (the line at 6645.13 Å is severely blended). Spectrum-synthesis calculations return an abundance of $\log \epsilon(\text{Eu}) = 0.04$; Eu is overabundant with $[\text{Eu}/\text{Fe}] = +1.35$.

Erbium (Er) Two lines of Er II are identified, 4759.671 Å and 4820.354 Å. Er abundances listed in Table 7 is estimated from spectrum synthesis calculation of 4759.671 Å line. The line parameters adopted from Kurucz atomic line list come from Meggers et al. (1975). Er shows an overabundance with $[\text{Er}/\text{Fe}] = +2.06$. Lawler et al. (2008) derived Er abundances in five very metal-poor, r-process-rich giant stars, CS 22892-052, BD +17 3248, HD 221170, HD 115444 and CS 31082-001 and found that the average Er abundance for the first four r-process-rich stars is slightly above the scaled (relative to Eu) solar value. For CS 31082-001, Lawler et al. derived $\log \epsilon(\text{Er}) = -0.30 \pm 0.01$ and $\log \epsilon(\text{Eu}/\text{Er}) = -0.42$ which is similar to Eu/Er ratios found for the other four giants. Estimated Er abundance in CS 29497-030, a star rich in both r- and s-process material is found to be $\log \epsilon(\text{Er}) = -0.57 \pm 0.02$ and $\log \epsilon(\text{Eu}/\text{Er}) = -0.62$. The 0.2 dex difference in the ratio between this star and the other five stars is interpreted as a result of the effects of changing from pure *r* abundance to a mix of *r* + *s*. This value for HD 209621 is ~ -1.1 . Lawler et al. did not use the line at 4759.671 Å, this line is listed in Kurucz atomic line list. The Er abundances do not show noticeable dependence on wavelength, $\log(gf)$, or on excitation potential (Lawler et al. 2008).

Tungsten (W) Three lines of W I 4757.542 Å, 5793.036 Å and 5864.619 Å are identified. The line used to derive the W abundance is 4757.542 Å. The abundance derived is high with $[\text{W}/\text{Fe}] = 2.61$; there is a possible blend with Cr I line at 4757.578 Å (with $\log g$ and lower excitation potential, -0.920 and 3.55 respectively) resulting in an overestimate of W abundance.

Lead (Pb) Spectrum-synthesis calculation is also used to determine the abundance of Pb using the Pb I line at 4057.8 Å. This line is strongly affected by molecular absorption of CH. CH lines are included in our spectrum synthesis calculation.

REFERENCES

- Abia, C., Dominguez, I., Gallino, R., Busso, M., Masera, S., Staniero, O., de Laverny, P., Plez, B. & Isern, J., 2002, ApJ, 579, 817
- Alonso A., Arribas S., Martinez-Roger C., 1996 A&A, 313, 873
- Alonso A., Arribas S., Martinez-Roger C., 1999, A&AS, 140, 261
- Aoki, W., Ryan, S. G., Norris, J. E., Beers T. C., Ando H., Iwamoto N., Kajino T., Mathews G. J., Fujimoto M. Y., 2001, ApJ, 561, 346
- Aoki, W., Ryan, S. G., Norris, J. E., Beers, Timothy C., Hiroyasu, A., Tsangarides, S. 2002, ApJ, 580, 1149
- Arlandini, C., Käppeler, F., Wisshak, K., Gallino, R., Lugaro, M., Busso, M., Straniero, O., 1999, ApJ, 525, 886
- Asplund M., Grevesse N., Sauval A. J., 2005, ASPC, 336, 25
- Bo Zhang, Kun Ma and Zhou Guide, 2006, ApJ, 642, 1075
- Howard, W. M., Mathews, G. J., Takahashi K., Ward, R. A., 1986, ApJ, 309, 633
- Barbuy B., Spite M., Spite F., Hill V., Cayrel R., Plez B., Petitjean P., 2005, A&A, 429, 1031
- Bartkevicius A., 1996, BaltA, 5, 217
- Baumüller D., Butler K., Gehren T., 1998, A&A, 338, 637
- Baumüller D., Gehren T., 1997, A&A, 325, 1088
- Beers T. C., Christlieb N., 2005, ARAA, 43, 561
- Bergeat J, Knapik A., Rutily B., 2001, A&A, 369, 179
- Bessell M. S., Brett J. M., 1988, PASP, 100, 1134
- Biemont E., Grevesse N., Hannaford P., Lowe R. M., 1981, ApJ, 248, 867
- Carpenter J, M., 2001, AJ, 121, 2851
- Cayrel R., Depagne E., Spite M., Hill V., Spite F., Francois P., Plez B., Beers T. C., Primas F., Andersen J. et al. 2004, A&A, 416, 1117
- Climenhaga J. L., 1960, Publ. DAO, 11, 307
- Corliss C. H., Bozman W. R., 1962, NBS Monograph 53
- Fuhr J. R., Martin G. A., Wiese W. L., 1988, J. Phys. Chem. Ref. Data, 17, Suppl. 4
- Goriely S., Mowlavi, N., 2000, A&A, 362, 599
- Goswami A. 2005, MNRAS, 359, 531
- Goswami A., Prantzos N., 2000, A&A, 359, 191
- Goswami A., Wako A., Beers T. C., Christlieb N., Norris J., Ryan S. G., Tsangarides S. 2006, MNRAS, 372, 343
- Goswami A., Bama P., Shantikumar, N. S., Devassy D. 2007, BASI, 35, 339
- Goswami A., Karinkuzhi D., Shantikumar, N. S., 2010, MNRAS, 402, 1111 (arXiv:0912.4347)
- Hill V., Barbuy B., Spite M., Spite F., Cayrel R., Plez B., Beers T. C., Nordström B., Nissen P. E., 2000, A&A, 353, 557
- Jonsell K., Barklem P.S., Gustafsson B., Christlieb N., Hill V., Beers T.C., Holmberg J., 2006, A&A, 451, 651
- Jonhson, J. A. & Bolte, M., 2002, ApJ, 579, L87
- Lambert D. L., Heath J. E., Lemke M., Drake J., 1996, ApJS, 103, 183
- Lawler J. E., Bonvallet G., Sneden C., 2001, ApJ, 556, 452
- Lawler J. E., Hartog E. A. Den, Sneden C., Cowan J. J., 2006, ApJS, 162, 227
- Lawler J.E., Sneden C., Cowan J. J., Wyart J.-F., Ivans I. L., Sobeck J. S., Stockett M. H., Den Hartog E. A., 2008, ApJS, 178, 71
- McClure R. D., 1983, ApJ, 268, 264
- McClure R. D., 1984, ApJ, 280, L31

McClure R. D., Woodsworth W., 1990, ApJ, 352, 709
Martin G. A., Fuhr J. R., Wiess, W. L., 1988, J. Phys. Chem.
Ref. data, 17, Suppl. 3
McWilliam A., 1990, ApJS, 74, 1075
McWilliam A., 1998, AJ, 115, 1640
McWilliam A., Preston G. W., Sneden C., Searle L., 1995a, AJ,
109, 2757
McWilliam A., Preston G. W., Sneden C., Sheckman S., 1995b,
AJ, 109, 2736
Meggers W. F., Corliss C. H., Scribner B. F., 1975, NBS Mono-
graph 145
Miles B. M., Wiese W. L., 1969, NBS Technical note 474
Noguchi K., Aoki W., Kawanomoto S., Ando H., Honda S., Izu-
miura H., Kambe E., Okita K. et al., 2002, PASJ, 54, 855
Obbarius, H. U., Kock M., 1982, J. Phys. B15, 527
Phillips J. G., Davis S. P., 1968, ZA, 69, 385
Preston G. W., Sneden C., 2001, AJ, 122, 1545
Platais I., Pourbaix D., Jorissen A., Makarov V. V., Berdnikov
L. N., Samus N. N., Lloyd Evans T., Lebzelter T., Sperauskas
J., 2003, A&A, 397, 997
Ryan S. G., Norris J. E., Beers T. C., 1996, ApJ, 471, 254
Sleivyte J., Bartkevicius A. 1990, Vilinius Astron. Obs. Bull., 85,
3
Skrutskie M. F., Cutri R. M., Stiening R., Weinberg M. D.,
Schneider S., Carpenter J. M., Beichman C., Capps R.,
Chester T., Elias J., et al., 2006, AJ, 131, 1163
Sneden C., 1973, PhD thesis, Univ of Texas at Austin
Sneden C., McWilliam A., Preston G. W., Cowan John J., Burris
D. L., Armosky B. J., 1996, ApJ, 467, 819
Stephens, A., 1999, AJ, 117, 1771
Tsuji T., Tomioka K., Sato H., Iye M., Okada T., 1991, A&A,
252, L1
Van Eck S., Goriely S., Jorissen, A., Plez, B. 2003, A&A, 404,
291
Vanture A. D., 1992a, AJ, 103, 2035
Vanture A. D., 1992b, AJ, 104, 1986
Vanture A. D., 1992c, AJ, 104, 1997
Wallerstein G., 1969, ApJ, 158, 607
Wheeler J. C., Sneden C., Truran J. W. Jr., 1989, ARAA, 27, 279